GEOLOGY | THE GEOLOGICAL SOCIETY OF AMERICA®

https://doi.org/10.1130/G49572.1

Manuscript received 9 August 2021
Revised manuscript received 14 December 2021
Manuscript accepted 20 December 2021

Published online 8 March 2022

Shallow distributed faulting in the Imperial Valley, California, USA

Valerie J. Sahakian[1], Boe J. Derosier[2], Thomas K. Rockwell[3] and Joann M. Stock[4]
[1]Department of Earth Sciences, University of Oregon, Eugene, Oregon 97403, USA
[2]Scripps Institution of Oceanography, University of California–San Diego, La Jolla, California 92037, USA
[3]Department of Geological Sciences, San Diego State University, San Diego, California 92182, USA
[4]Seismological Laboratory, California Institute of Technology, Pasadena, California 91125, USA

ABSTRACT

In the tectonically complex Imperial Valley, California (USA), the Imperial fault (IF) is often considered to be the primary fault at the U.S.-Mexico border; however, its strain partitioning and interactions with other faults are not well understood. Despite inferred evidence of other major faults (e.g., seismicity), it is difficult to obtain a holistic view of this system due to anthropogenic surface modifications. To better define the structural configuration of the plate-boundary strain in this region, we collected high-resolution shallow seismic imaging data in the All American Canal, crossing the Imperial, Dixieland, and Michoacán faults. These data image shallow (<25 m) structures on and near the mapped trace of the Imperial fault, as well as the Michoacán fault and adjacent stepover. Integration of our data with nearby terrestrial cores provides age constraints on Imperial fault deformation. These data suggest that the Michoacán fault, unmapped in the United States, is active and likely produces dynamic or off-fault deformation within its stepover to the Dixieland fault. Together, these data support more strain partitioning than previously documented in this region.

INTRODUCTION

North of the Gulf of California, along the Pacific–North America plate boundary, the Imperial Valley is a tectonically complex region (Larsen and Reilinger, 1991; Han et al., 2016). Strain is partitioned eastward into the Eastern California shear zone and subsequently north to the Walker Lane, an incipient Pacific–North American plate transform boundary (Dokka and Travis, 1990; Wesnousky, 2005). This leads to active fault evolution, interaction, and strain partitioning in the region (Crowell et al., 2013), which are important to understand for present-day fault interactions and seismic hazard, and to elucidate the history of this complex, segmented margin.

At the latitude of the U.S.-Mexico border, the Imperial fault (IF) is considered to be the major structure in the Pacific–North American plate-boundary system, hosting two large recent earthquakes (1940 **M** 7.0 and 1979 **M** 6.5; Trifunac and Brune, 1970; Archuleta, 1984). The Uniform California Earthquake Rupture Forecast version 3 (UCERF3, https://www.scec.org/ucerf; Field et al., 2014) hazard model attributes 30–40 mm/yr of plate-boundary slip to this fault. Geologic slip rates are much lower (15–20 mm/yr; Thomas and Rockwell, 1996). Patterns of seismicity in the Imperial Valley suggest that several other inferred faults share the plate-boundary strain with the IF, including the Weinert–El Centro, Dixieland (DF), and Michoacán (MF) faults (Magistrale, 2002; González-Escobar et al., 2020). Seismicity lineaments indicate that the MF extends north of the U.S.-Mexico border, accommodating some plate-boundary slip, as do joint interferometric synthetic aperture radar (InSAR) and global navigation satellite system (GNSS) studies, which place slip on a structure 10–20 km to the west of the IF (Lindsey and Fialko, 2016). Similarly, south of the border, geodetic data support shared slip among the IF, MF, and faults of the Sierra Cucapah, Mexico (Sandwell et al., 2016). Likewise, mechanical models (Dorsett et al., 2019) found that the MF/Cerro Prieto fault is likely linked to the IF system, and faults such as the DF accommodate some of the IF's strain, changing our understanding of fault interaction in the Imperial Valley.

Geomorphic evidence of faulting is, however, almost entirely obscured in the Imperial Valley due to anthropogenic activity and ancient Lake Cahuilla sediments, posing challenges in identifying suitable sites for geologic studies and paleoseismic trench campaigns. Although several trenches exist in the region (e.g., Thomas and Rockwell, 1996; Jerrett, 2016; Wessel, 2016), the slip rate of the IF is not as well constrained as other faults in Southern California. Without direct observations of shallow faulting, it is challenging to fully characterize these structures geologically.

DATA

We address this insufficiency of observations with a novel study to constrain young (<5 ka) deformation in the shallow subsurface. We used a traditionally marine subsurface imaging instrument in the All American Canal (AAC; Fig. 1), a large aqueduct that transports water from the Colorado River to the Imperial Valley. The All American Canal parallels the California-Mexico international border near Calexico, California, and directly crosses the IF, DF, and a proposed region of strain accommodation. With an acoustic compressed high-intensity radar pulse (CHIRP) instrument, we can attribute shallow deformation to these structures and further our understanding of the interaction of fault structures in the region. We towed the CHIRP from west to east through the All American Canal in a floating cage (Fig. 2). We collected 27 seismic lines in three main regions: near the (1) IF, (2) the DF, and (3) the inferred trace of the MF (3 in Fig. 1). Lines are abbreviated as ACDXXLYY, with XX indicating the day and YY indicating the line number. We approximated ages of the sediments with a sedimentation rate using calibrated ^{14}C dates from a nearby core (see the Supplemental Material[1]; Rockwell et al., 2019).

[1]Supplemental Material. Description of methods (seismic data processing, ^{14}C dating, interpretations, and Coulomb stress models), supplemental figures, and interpreted fault locations. Please visit https://doi.org/10.1130/GEOL.S.19104956 to access the supplemental material, and contact editing@geosociety.org with any questions. Data are stored at the Marine Geoscience Data System https://doi.org/10.26022/IEDA/330515.

CITATION: Sahakian, V.J., Derosier, B.J., Rockwell, T.K., and Stock, J.M., 2022, Shallow distributed faulting in the Imperial Valley, California, USA: Geology, v. XX, p. , https://doi.org/10.1130/G49572.1

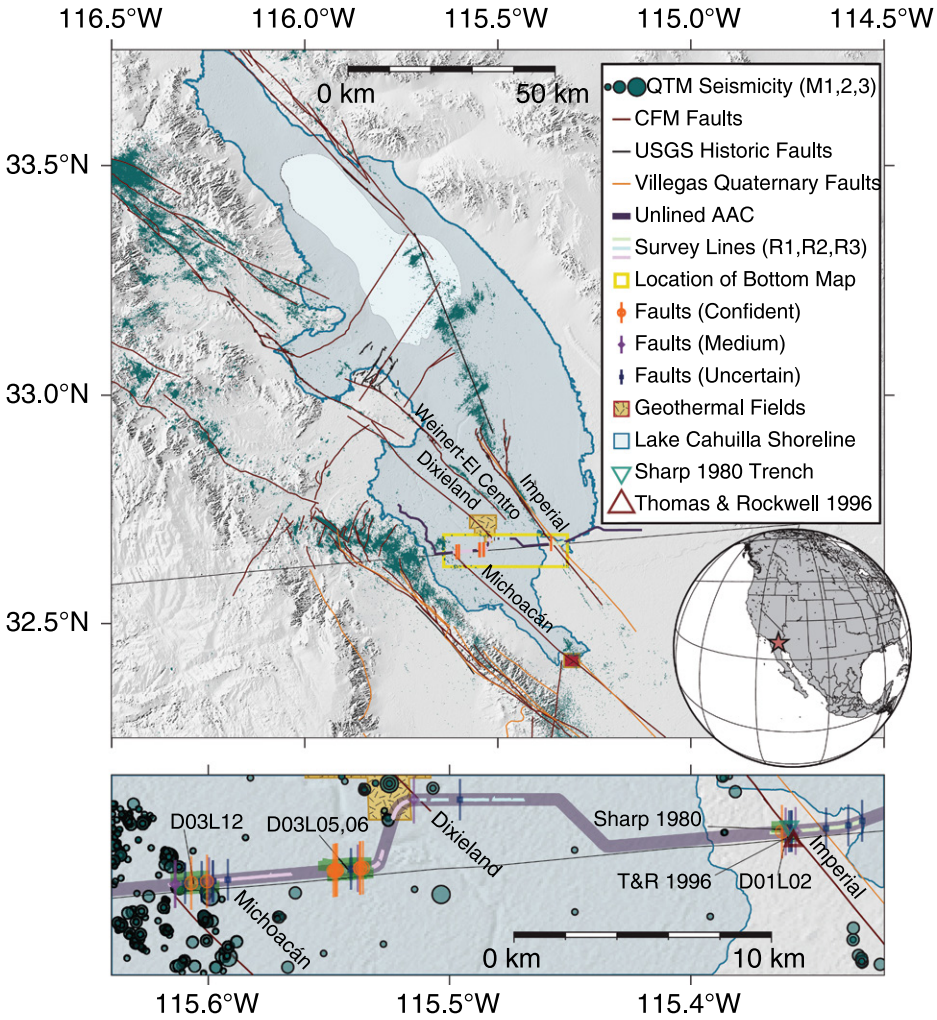

Figure 1. Top: Imperial Valley region of California, USA, showing the Southern California Earthquake Center community fault model (SCEC CFM 5.3) faults (Plesch et al., 2020), U.S. Geological Survey (USGS) historic faults (USGS, 2017), and Mexico Quaternary faults (Villegas et al., 2017), "confident" mapped faults from this study, quake template matching (QTM) 9.5 standard deviation database seismicity (Ross et al., 2019), select geothermal fields (Heber—yellow; Cerro Prieto—red), the unlined All American Canal (AAC), the trenches of Sharp (1980) and Thomas and Rockwell (1996; T&R 1996), and ancient Lake Cahuilla footprint (Buckles et al., 2002), as described in the legend. Inset: Red star on globe indicates map location. Yellow box indicates location of bottom map. Bottom: Survey region. In addition to the main map features, this study's survey lines are shown, as well as "medium" and "uncertain" mapped faults in this study, and earthquakes scaled by magnitude (legend). Seismic lines are highlighted in green with labels.

RESULTS

We characterized our interpretations as "confident," "medium confident," and "uncertain." Intermittent striping from gas throughout the dataset prevented local data interpretation in some places (Sahakian et al., 2016).

In region 1 (IF), only line ACD01L02 showed clear data. We observed deformation of thick, strong reflectors at 15–25 m depth assuming 1500 m/s water velocity (horizon 2, 5.4° dip), and less prominent reflectors beneath the canal bed forms, such as "shallow IF" (Fig. 3), with an apparent 3.4° dip to the west, intersected by the mapped traces of the IF (Nicholson et al., 2020; Plesch et al., 2020; Rockwell and Klinger, 2013). At ~0.4 km distance, there were small discontinuities in this reflector ("uncertain"), with gas obfuscation to the east. At ~0.17 km distance, we observed small offsets in reflectors (0.018–0.302 s) such as horizon 1, and at ~0.04 km. Underlying strata fold in toward an inferred structure ("confident"; Fig. 3). Other lines in region 1 exhibited thick, bright, flat-lying reflectors at the same depth.

In region 2 (DF), we observed some shallow deformation and folding of reflectors above 10 m depth; however, the reflectors were thinner and less continuous compared to region 1. Identifying surface offsets here was challenging due to high canal floor reflectivity. Multiples dominated >15 m, obscuring deformation below ~10 m. Most observable reflectors in this region were flat-lying. The mapped trace of the DF intersects day 2 line 1 (ACD02L01; Figs. S1 and S2), but interpretations were not possible due to the strong prevalence of gas.

Clear offsets and deformed reflectors were observed in region 3 (MF) on lines ACD03L05, ACD03L06, ACD03L12 (Fig. 4; Fig. S3), and ACD03L13 (Figs. S4 and S5). North of the mapped MF trace (ACD03L12), we observed clear offsets in reflectors (horizon 1) with down-to-the-west vertical separation of ~4.5 m. At ~1.1 km distance, there is an abrupt transition between continuous and chaotic reflectors ("confident"). There is a prominent region of gas in the middle of this line, separating flat-lying from dipping reflectors, likely due to a fault ("uncertain," ~0.9 km distance). The "confident" fault interpreted at ~0.2 km distance on ACD03L05 demonstrates reflector offset >1 m. An adjacent fault warps reflectors, but their continuity is not sufficient to confidently describe an offset. The eastern portion of ACD03L05 showed folded reflectors, and the adjoining ACD03L06 showed divergence of reflectors, small offsets, and a westward dip between two confidently mapped faults. Gas on line ACD03L13 occurred in the middle of the line, with reflectors dipping and thickening toward the center region of gas, potentially obscuring a structure responsible for this deformation ("uncertain").

DISCUSSION

The deformation in region 1 coincides with the mapped IF trace, likely representing IF deformation from the 1940 and previous earthquakes. Both the deep and shallow strata surrounding the mapped fault trace exhibit an apparent southwestward dip, which increases slightly with depth. Consistent with syndepositional faulting, this suggests a local, consistent sense of motion on the IF.

Obtaining a sedimentation rate here is fraught with uncertainties, but we aimed to place highly approximate temporal constraints on subsurface deformation. The All American Canal is 1 km south of a cone penetrometer (CPT) profile obtained by Rockwell et al. (2019) yielding stratal relationships, with two cores within and adjacent to the IF. Both cores, located on a berm at 9 m above sea level (1 m above the surrounding agricultural fields, averaging 8 m elevation), sampled several Holocene clay layers beneath interpreted ancient Lake Cahuilla Lake G deposits, with age control based on radiocarbon dating of mollusk shells, charcoal, and ostracods. The oldest sampled layer is ~16 m below sea level. In our data just 1 km to the south, the local canal water level from CHIRP-mounted GNSS is 8 m above sea level and 3 m below average land surface, suggesting that sedimentation should be consistent across this flat region.

With the cores, we estimated a sedimentation rate of 4.6–19 m/k.y. (>10 m depth), and an earlier rate of 3.6–5.7 m/k.y. (5–10 m). We thus estimated horizon 2 line ACD01L02 at ~0.03 s

Figure 2. Photos of compressed high-intensity radar pulse (CHIRP) instrument deployment. (A) Transducers on CHIRP bottom. (B) CHIRP frame. (C) Buoyant pontoons to float frame. (D) Deployment of CHIRP from northern canal bed. (E) Towing CHIRP from the southern bank with a towline; umbilical and second towline (right) toward the northern bank and topside. Global navigation satellite system (GNSS) receiver on frame mount (red circle and arrow). (F) Topside system setup.

two-way traveltime (TWTT; ~17.5–22.5 m beneath instrument, ~9.5–14.5 m below sea level) to be ca. 3.6–1.9 ka. See the Supplemental Material for additional information. Most deformation we observed in ACD01L02 is likely occurring in Holocene sediments, and the deepest antiformal deformation at ~2 km along-track distance is older, likely Pleistocene in age. The apparent southwestward tilt on the eastern portion of the line at ~4–6 m depth is likely <1.1 ka in age and is similar to the southwestward tilted strata noted in a nearby trench by Sharp (1980), but not by Thomas and Rockwell (1996) 75 m to the south (Fig. S6). This suggests that these structures may be produced by a local structural pressure ridge or pull-apart feature associated with a fault stepover. The fault we observed at ~0.17 km distance does not deform reflectors above ~0.0125 s TWTT, corresponding to <2.5 ka, or lakes below Lake G (ca. 2 ka; Rockwell et al., 2011), which implies that there have been no coseismic offsets on this structure for at least the last 3–4 IF events. This agrees with an analysis of aerial imagery of the

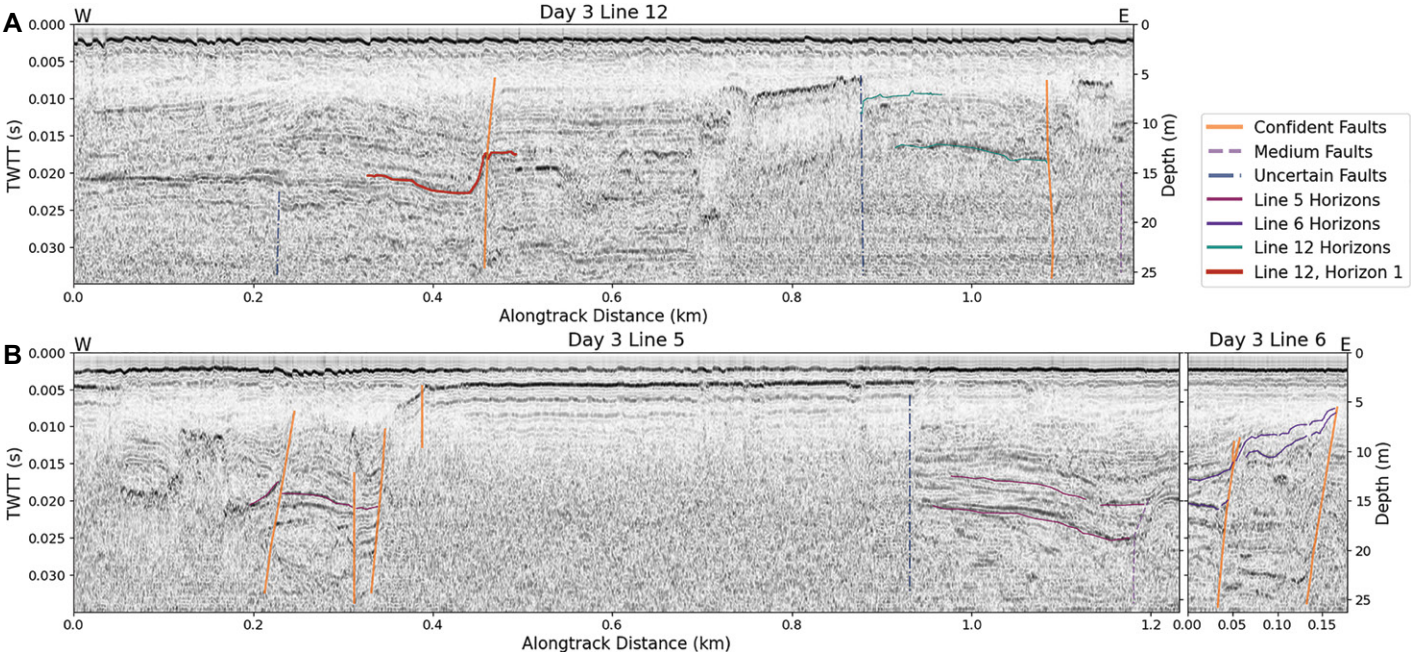

Figure 3. Data crossing the Imperial fault (IF, California, USA). Day 1 line 2 seismic line, showing deformation near mapped trace of the IF. Two-way traveltime (TWTT) is on the left axis, and depth below instrument is on the right axis. (A) Uninterpreted seismic profile. (B) Interpreted seismic profile. Faults are from the Southern California Earthquake Center (SCEC) Community Fault Model (CFM 5.3), U.S. Geological Survey (USGS) historic faults, and Rockwell and Klinger (2013) (RK13), as well as interpretations from this study. Select horizons and their names are indicated in the legend.

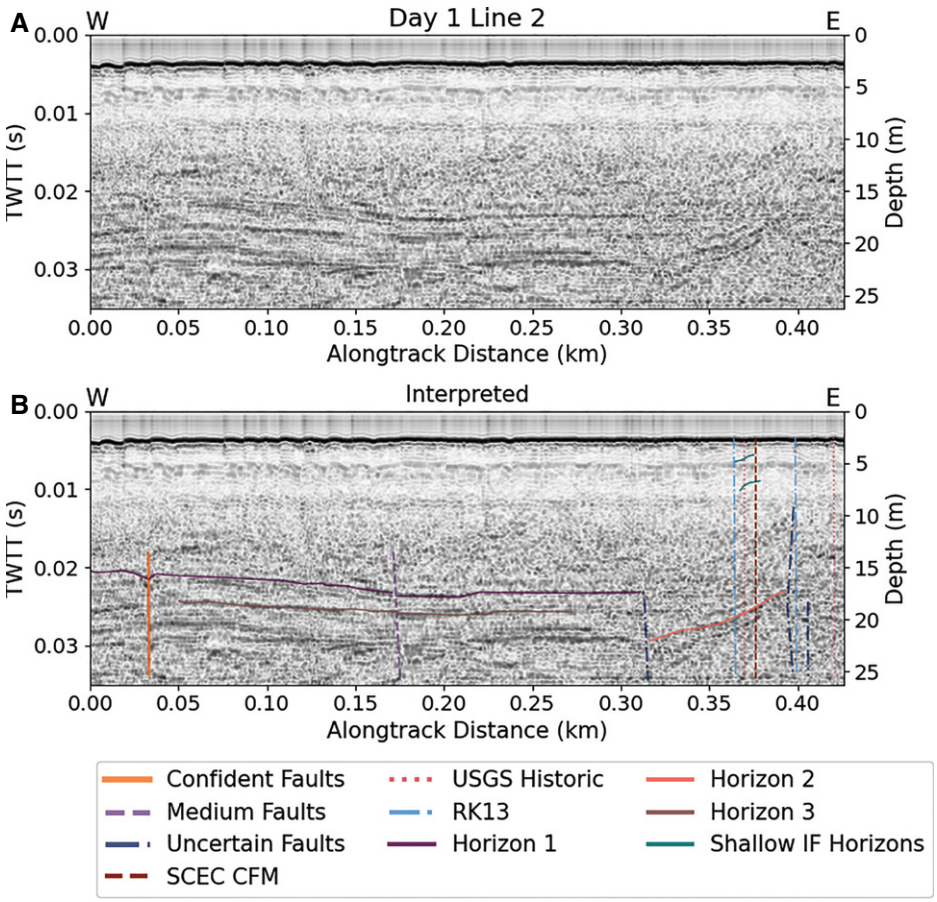

Figure 4. (A) Day 3 line 12 showing deformation and offset near the proposed Michoacán fault. Two-way traveltime (TWTT) is on the left axis, and depth below instrument is on the right axis. Line 12, horizon 1 reflector shows ~4.5 m of vertical offset next to the mapped fault. (B) Day 3 lines 5 and 6 (~15 m apart) showing deformation between the Michoacán and Dixieland faults.

1940 Imperial Valley earthquake (Rockwell and Klinger, 2013), where we also found no evidence of surface offsets near this structure along its strike to the northwest and southeast in agricultural fields with closely spaced crop rows.

Region 3 shows the most compelling evidence of shallow deformation and provides the first-ever evidence of shallow faulting in this region to the west of the IF. We documented two distinct locations with faulting. The first is within the postulated location of the northern extension of the MF. The offsets on reflectors here are comparable to, if not larger than, those observed across the IF in region 1 (Figs. 3 and 4). The second evidence of faulting is farther east, on lines ACD03L05 and ACD03L06. We interpret transtensional faulting features here, both at greater depths and in the shallow subsurface, though we could not resolve surface faulting in these strata.

Our observations of shallow faulting in the westernmost section of region 3 are not unexpected, as others have proposed that the MF likely extends to the north, and that the DF accommodates some plate-boundary strain here (Magistrale, 2002; Lin, 2013). Dorsett et al. (2019) found that the MF and Cerro Prieto fault are likely linked to the IF system, and that the adjacent DF accommodates ~3–8 mm/yr of slip, repartitioning some of the UCERF3 IF slip rate onto the DF and MF. Furthermore, Lindsey and Fialko (2016) placed 10–15 mm/yr of slip on an unnamed structure(s) at this latitude, which may be in part accommodated by the MF. We thus propose that the deformation on lines ACD03L12 is the shallow manifestation of slip associated with the northern extension of the MF, which is also observable in seismicity. This structure is yet to be geologically investigated north of the U.S.-Mexico border, and it is not included in current fault models.

The transtensional structures on lines ACD03L05 and ACD03L06 may be associated with a small basin postulated by previous workers in the area (Persaud et al., 2016). However, there is no observed seismicity in comprehensive seismic catalogs (Fig. 1) within the wide (~10 km) stepover between the MF and DF (Ross et al., 2019). Other similar regional young and active basins, such as the Mesquite basin, exhibit shallow faulting and deformation and host active seismicity (Rockwell and Meltzner, 2008; Brothers et al., 2009). We propose four possible hypotheses for the presence of shallow faulting in this region:

(H1) A mature, strain-accommodating fault exists at depth, but it is in the stress shadow of the 2010 El Mayor–Cucapah or 1979 Imperial Valley earthquakes.

(H2) There is no main structure in this region; rather, these shallow features represent coseismic offsets from through-going rupture within the stepover.

(H3) The faulting is due to coseismic offsets from rupture on either the MF or the DF that dynamically propagated into but not through the stepover, and this activity was associated with the formation of a small local basin.

(H4) The transtensional structures we observe are from a relic fault system (the MF or DF), from which activity moved to the west or east over time.

Simple models of Coulomb stress change (Figs. S7 and S8) in the region from the 1979 Imperial Valley and 2010 El Mayor–Cucapah earthquakes can test H1. The stepover does not preferentially experience an increase or decrease in stress compared to the observed seismicity lineaments, which implies that the absence of seismicity is not likely due to static stress changes. It is not possible for us to propose any further constraints on the possibility of through-going rupture (H2) with our data set; however, we posit that this is improbable—a stepover of 10 km width is highly unlikely to allow for through-going rupture (Biasi and Wesnousky, 2016). We cannot distinguish between H3 and H4 with our data set; however, both seem plausible, given the documented possibility for propagating ruptures to trigger slip on preexisting or new structures within a radius near the rupture front (Wesnousky, 2008), and for off-fault deformation to occur statically or dynamically near a large rupture or mature fault (Milliner et al., 2015; Okubo et al., 2020). Further work would be necessary to characterize the three-dimensional nature of these offsets and their timing, and to understand if they represent active fault evolution and interaction, or if they represent dynamically triggered offsets within this stepover.

CONCLUSIONS

Our novel terrestrial application of CHIRP provides the first images of subsurface deformation across structures in the Imperial Valley, including the Imperial fault and Michoacán fault. It confirms that the Michoacán fault/Cerro Prieto fault extends northward into the United States. We observed transtensional structures in the region between the Michoacán fault and Dixieland fault, potentially coseismic displacements in the stepover between these faults, and a relic fault system. We cannot place slip rates on these faults based solely on two-dimensional imagery and lack direct dating of the imaged strata. Nevertheless, this work provides valuable constraints for the locations of future studies to understand regional strain distribution, slip rates, and fault interactions in the Imperial Valley.

ACKNOWLEDGMENTS

This work was funded by Southern California Earthquake Center grant #18119. We thank Neal Driscoll for the use of his CHIRP; Alistair Harding for discussions regarding the seismic data; Ray Weldon and Becky Dorsey for feedback; Brian Oller and Alexis Klimasewski for help with data collection; Socrates Gonzalez and Robert Pacheco (Imperial Irrigation District], Imperial, California) for their support of the study; and many other IID employees who gave their time to aid in data collection. We thank Aron Meltzner, an anonymous reviewer, and editor William Clyde for their thorough reviews, which improved this manuscript.

REFERENCES CITED

Archuleta, R.J., 1984, A faulting model for the 1979 Imperial Valley earthquake: Journal of Geophysical Research: Solid Earth, v. 89, B6, p. 4559–4585, https://doi.org/10.1029/JB089iB06p04559.

Biasi, G.P., and Wesnousky, S.G., 2016, Steps and gaps in ground ruptures: Empirical bounds on rupture propagation: Bulletin of the Seismological Society of America, v. 106, p. 1110–1124, https://doi.org/10.1785/0120150175.

Brothers, D.S., Driscoll, N.W., Kent, G.M., Harding, A.J., Babcock, J.M., and Baskin, R.L., 2009, Tectonic evolution of the Salton Sea inferred from seismic reflection data: Nature Geoscience, v. 2, p. 581–584, https://doi.org/10.1038/ngeo590.

Buckles, J.E., Kashiwase, K., and Krantz, T., 2002, Reconstruction of prehistoric Lake Cahuilla in the Salton Sea Basin using GIS and GPS: Hydrobiologia, v. 473, p. 55–57, https://doi.org/10.1023/A:1016513214122, https://hub.arcgis.com/datasets/ac2b6de1149047b9af934acd4d01fdca/about.

Crowell, B.W., Bock, Y., Sandwell, D.T., and Fialko, Y., 2013, Geodetic investigation into the deformation of the Salton Trough: Journal of Geophysical Research: Solid Earth, v. 118, p. 5030–5039, https://doi.org/10.1002/jgrb.50347.

Dokka, R.K., and Travis, C.J., 1990, Role of the Eastern California shear zone in accommodating Pacific–North American plate motion: Geophysical Research Letters, v. 17, p. 1323–1326, https://doi.org/10.1029/GL017i009p01323.

Dorsett, J.H., Madden, E.H., Marshall, S.T., and Cooke, M.L., 2019, Mechanical models suggest fault linkage through the Imperial Valley, California, USA: Bulletin of the Seismological Society of America, v. 109, p. 1217–1234, https://doi.org/10.1785/0120180303.

Field, E.H., Arrowsmith, R.J., Biasi, G.P., Bird, P., Dawson, T.E., Felzer, K.R., et al., 2014, Uniform California Earthquake Rupture Forecast, version 3 (UCERF3)—The time-independent model: Bulletin of the Seismological Society of America, v. 104, p. 1122–1180, https://doi.org/10.1785/0120130164.

González-Escobar, M., Agüero, M.A.M., and Martin, A., 2020, Subsurface structure revealed by seismic reflection images to the southwest of the Cerro Prieto pull-apart basin, Baja California: Geothermics, v. 85, p. 101779, https://doi.org/10.1016/j.geothermics.2019.101779.

Han, L., Hole, J.A., Stock, J.M., Fuis, G.S., Kell, A., Driscoll, N.W., et al., 2016, Continental rupture and the creation of new crust in the Salton Trough rift, Southern California and northern Mexico: Results from the Salton Seismic Imaging Project: Journal of Geophysical Research: Solid Earth, v. 121, p. 7469–7489, https://doi.org/10.1002/2016JB013139.

Jerrett, A.S., 2016, Paleoseismology of the Imperial Fault at the US-Mexico Border, and Correlation of Regional Lake Stratigraphy Through Analysis of Oxygen/Carbon Isotope Data [M.S. thesis]: San Diego, California, San Diego State University, 107 p., https://digitallibrary.sdsu.edu/islandora/object/sdsu%3A1764.

Larsen, S., and Reilinger, R., 1991, Age constraints for the present fault configuration in the Imperial Valley, California: Evidence for northwestward propagation of the Gulf of California rift system: Journal of Geophysical Research: Solid Earth, v. 96, B6, p. 10339–10346, https://doi.org/10.1029/91JB00618.

Lin, G., 2013, Three-dimensional seismic velocity structure and precise earthquake relocations in the Salton Trough, Southern California: Bulletin of the Seismological Society of America, v. 103, p. 2694–2708, https://doi.org/10.1785/0120120286.

Lindsey, E.O., and Fialko, Y., 2016, Geodetic constraints on frictional properties and earthquake hazard in the Imperial Valley, Southern California: Journal of Geophysical Research: Solid Earth, v. 121, p. 1097–1113, https://doi.org/10.1002/2015JB012516.

Magistrale, H., 2002, The relation of the southern San Jacinto fault zone to the Imperial and Cerro Prieto faults, *in* Barth, A., ed., Contributions to Crustal Evolution of the Southwestern United States: Geological Society of America Special Paper 365, p. 271–278, https://doi.org/10.1130/0-8137-2365-5.271.

Milliner, C.W., Dolan, J.F., Hollingsworth, J., Leprince, S., Ayoub, F., and Sammis, C.G., 2015, Quantifying near-field and off-fault deformation patterns of the 1992 M_w 7.3 Landers earthquake: Geochemistry Geophysics Geosystems, v. 16, p. 1577–1598, https://doi.org/10.1002/2014GC005693.

Nicholson, C., Plesch, A., Sorlien, C.C., Shaw, J.H., and Hauksson, E., 2020, Updates, evaluation and improvements to the Community Fault Model (CFM version 5.3): Poster Presentation #182 at the 2020 SCEC Annual Meeting: Los Angeles, Southern California Earthquake Center, Contribution 10412.

Okubo, K., Rougier, E., Lei, Z., and Bhat, H.S., 2020, Modeling earthquakes with off-fault damage using the combined finite-discrete element method: Computational Particle Mechanics, v. 7, p. 1057–1072, https://doi.org/10.1007/s40571-020-00335-4.

Persaud, P., Ma, Y., Stock, J.M., Hole, J.A., Fuis, G.S., and Han, L., 2016, Fault zone characteristics and basin complexity in the southern Salton Trough: California Geology, v. 44, p. 747–750, https://doi.org/10.1130/G38033.1.

Plesch, A., Marshall, S.T., Nicholson, C., Shaw, J.H., Maechling, P.J., and Su, M., 2020, The Community Fault Model version 5.3 and new web-based tools: Poster Presentation #184 at the 2020 SCEC Annual Meeting: Los Angeles, Southern California Earthquake Center Contribution 10547.

Rockwell, T.K., and Klinger, Y., 2013, Surface rupture and slip distribution of the 1940 Imperial Valley earthquake, Imperial fault, Southern California: Implications for rupture segmentation and dynamics: Bulletin of the Seismological Society of America, v. 103, p. 629–640, https://doi.org/10.1785/0120120192.

Rockwell, T.K., and Meltzner, A.J., 2008, Non-characteristic slip and earthquake clustering on the Imperial fault, Mesquite Basin, Imperial Valley, California: San Francisco, California, American Geophysical Union, Fall Meeting supplement, abstract T11A–1845.

Rockwell, T.K., Meltzner, A., and Tsang, R., 2011, A Long Record of Earthquakes with Timing and Displacements for the Imperial Fault: A Test of Earthquake Recurrence Models: U.S. Geological Survey Final Technical Report Grant No. 15-HQ-G10AP00003, 28 p., https://earthquake.usgs.gov/cfusion/external_grants/reports/G10AP00003.pdf.

Rockwell, T., Klinger, Y., Wessel, K.N., and Jerrett, A., 2019, Testing Recurrence Models for a Simple Plate Boundary Fault: Paleoseismic Study of the Imperial Fault in the Region of Large 1940 Displacement: U.S. Geological Survey Final Technical Report Grant No. 15-HQ-G15AP00010, 34 p., https://earthquake.usgs.gov/cfusion/external_grants/reports/G15AP00010.pdf.

Ross, Z.E., et al., 2019, Hierarchical interlocked orthogonal faulting in the 2019 Ridgecrest earthquake sequence: Science, v. 366, p. 346–351, https://doi.org/10.1126/science.aaz0109.

Sahakian, V., Kell, A., Harding, A., Driscoll, N., and Kent, G., 2016, Geophysical evidence for a San Andreas subparallel transtensional fault along the northeastern shore of the Salton Sea: Bulletin of the Seismological Society of America, v. 106, p. 1963–1978, https://doi.org/10.1785/0120150350.

Sandwell, D., Gonzalez-Ortega, A., Gonzalez, J., and Thatcher, W., 2016, Assembly of the Community Geodetic Model and GPS Survey of the Cerro Prieto Fault: Southern California Earthquake Center Annual Report, Report 16072, https://files.scec.org/s3fs-public/reports/2016/16072_report.pdf.

Sharp, R.V., 1980, 1940 and prehistoric earthquake displacements on the Imperial fault, Imperial and Mexicali Valleys, California and Mexico, *in* California Seismic Safety Commission Symposium Proceedings, The Human Settlements on the San Andreas Fault: Sacramento, California, California Seismic Safety Commission, p. 68–81.

Thomas, A.P., and Rockwell, T.K., 1996, A 300- to 550-year history of slip on the Imperial fault near the US-Mexico border: Missing slip at the Imperial fault bottleneck: Journal of Geophysical Research: Solid Earth, v. 101, B3, p. 5987–5997, https://doi.org/10.1029/95JB01547.

Trifunac, M.D., and Brune, J.N., 1970, Complexity of energy release during the Imperial Valley, California, earthquake of 1940: Bulletin of the Seismological Society of America, v. 60, p. 137–160, https://doi.org/10.1785/BSSA0600010137.

U.S. Geological Survey, 2017, Quaternary Fault and Fold Database for the United States: https://www.usgs.gov/natural-hazards/earthquake-hazards/faults (accessed 1 August 2017).

Villegas, G.C., Mendoza, C., and Ferrari, L., 2017, Base de datos de fallas cuaternarias de México: Terra Digitalis, v. 1, https://doi.org/10.22201/igg.terradigitalis.2017.1.3.

Wesnousky, S.G., 2005, Active faulting in the Walker Lane: Tectonics, v. 24, TC3009, https://doi.org/10.1029/2004TC001645.

Wesnousky, S.G., 2008, Displacement and geometrical characteristics of earthquake surface ruptures: Issues and implications for seismic-hazard analysis and the process of earthquake rupture: Bulletin of the Seismological Society of America, v. 98, p. 1609–1632, https://doi.org/10.1785/0120070111.

Wessel, K.N., 2016, 500 Year Rupture History of the Imperial Fault at the International Border through Analysis of Faulted Lake Cahuilla Sediments, ^{14}C Data, and Climate Data [M.S. thesis]: San Diego, California, San Diego State University, 73 p., https://digitallibrary.sdsu.edu/islandora/object/sdsu%3A1832.

Printed in USA